



Bruno R. Cotrim · Aurélio L. Araújo · José F. A. Madeira

# Optimal resistive shunted damping configurations for multi-modal noise reduction in sandwich panels

Received: 16 November 2021 / Accepted: 10 October 2022 / Published online: 2 November 2022  
© The Author(s), under exclusive licence to Springer-Verlag GmbH Austria, part of Springer Nature 2022

**Abstract** This paper looks into the issue of noise attenuation in sandwich panels using a viscoelastic core and piezoelectric patches with an associated resistive (R) circuit. The laminated sandwich panel is modeled using an in-house finite element code from which the frequency response of the panel is calculated that is then used to calculate the radiated sound power by the Rayleigh integral method. The optimal location for the patches, as well as the values for the associated resistors, is obtained by a 7-objective optimization problem using the Direct MultiSearch algorithm, minimizing the added weight, number of equipotential zones, and the noise radiated for the first five modes. A Pareto optimal front is obtained with optimal patch distribution and resistance (R) values for each equipotential zone.

## 1 Introduction

The use of composite materials is growing in the aerospace and automotive industries due to their good mechanical properties while being much lighter than the metals they are currently replacing. This weight reduction leads to less energy required which in turn leads not only to a decrease in fuel usage, but also to an increase in the performance of the structures/dynamic systems. However, the mass reduction comes at a cost of a higher susceptibility to acoustic problems when these structures are subjected to external mechanical or acoustic excitations. Multiple active and passive damping technologies can be employed in order to reduce the levels of acoustic emissions of the structure, for example, the use of viscoelastic materials and shunted piezoelectric networks [1]. Since viscoelastic materials work better at higher frequencies and shunted damping circuits work better for lower frequencies, as the loss factor is higher in different frequency ranges for each technology, these two technologies can be combined using sandwich plates.

The use of piezoelectric materials along with resistance–inductance (RL) shunt circuits for structural damping was first suggested and implemented experimentally by Forward [2]. The first calibration procedure for RL serial circuits was proposed by Hagood and van Flotow [3] considering the mechanical impedance of the structure. Few years later, Wu [4] developed a calibration method for parallel circuits using the same approach. Since then, other authors have developed new calibration methods, with Tang [5] adding a negative

---

B. R. Cotrim (✉) · A. L. Araújo · J. F. A. Madeira  
IDMEC, Instituto Superior Técnico, Universidade de Lisboa, Av. Rovisco Pais, 1, 1049-001 Lisboa, Portugal  
E-mail: brunocotrim@tecnico.ulisboa.pt

A. L. Araújo  
E-mail: aurelio.araujo@tecnico.ulisboa.pt

J. F. A. Madeira  
E-mail: aguilarmadeira@tecnico.ulisboa.pt

J. F. A. Madeira  
ADM, ISEL, Instituto Politécnico de Lisboa, Rua Conselheiro Emídio Navarro, 1, 1959-007 Lisboa, Portugal

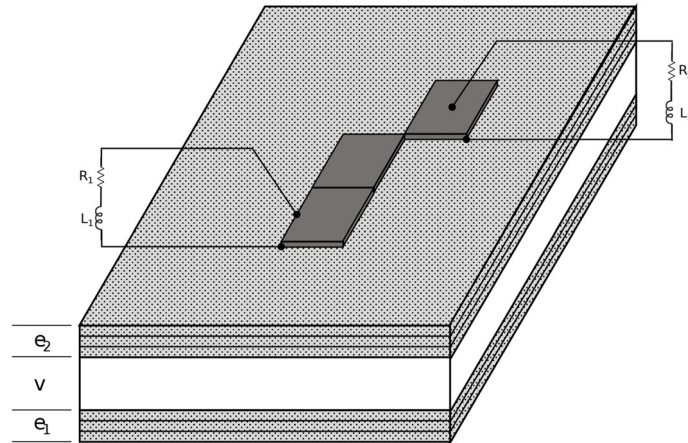


**Fig. 1** The sandwich plate with a piezoelectric patch and its associated RL shunted circuit

capacitance to improve the electromechanical coupling effect, and more recently Toftekær et al. [6] have proposed a calibration method with residual mode correction.

Some authors have in the past addressed the issue regarding active and passive noise reduction in composite structures. The work done by Larbi et al. [7–12] analyzes the structural–acoustic problems with smart piezoelectric composite and sandwich plates with and without a viscoelastic core. The passive control has recently been approached by Vieira and Araújo [13], where the stacking sequence was optimized and then the patch configuration. The same authors have also implemented active control for noise reduction using a PID controller implemented in ANSYS [14].

This paper is a further development of the work presented by Araújo and Madeira [15], where a layer-wise sandwich finite element code was implemented with a frequency-dependent viscoelastic core composite laminated skin layer and piezoelectric patches being placed in the top surface of the panel with an associated resistive circuit. A multi-objective problem was solved in order to obtain the optimal patch configuration for noise and vibration damping tackling multiple modes at the same time, with a total of five objectives: minimize the mass, the number of equipotential zones, and the noise radiated in the three highest peaks across a specific frequency range, where the radiated sound power (RSP) is used as the acoustic indicator. The new idea is, instead of tackling the modes indiscriminately, to target specific modes (in this case, the first five), thus allowing to obtain solutions that can either target one of them individually or that can reduce their overall response. Likewise, the same solver, Direct MultiSearch (DMS), is used in this work.

DMS [16] is a numerical solver for multi-objective optimization that does not require the computation of objective function derivatives nor aggregates the objective functions. The method was developed as a generalization of the single-objective optimization method direct search. Regarding its application to improve the acoustic performance of laminated sandwich panels, it has been previously used to maximize the loss factor while minimizing only the weight [17] and then both the weight and material cost [18], with the latter application being the 5 objective problem [15] described in the previous paragraph.

## 2 Sandwich plate model

In this Section, the layer-wise sandwich laminated plate model is presented. It is comprised by two composite laminated face layers, ( $e_1$ ) and ( $e_2$ ), a viscoelastic core, ( $v$ ), and piezoelectric patches, ( $p$ ), bonded to the top outer surface of the plate (Fig. 1).

An RL shunted circuit is connected to each piezoelectric layer with an inductance and a resistance mounted in series [3]. The general idea is for the mechanical energy of the plate to be converted to electrical energy in the piezoelectric patch, that works as an electrical capacitance, which is then dissipated in the resistance as heat. The inductance synchronizes both the plate and circuit resonant frequencies. Although in this work the inductors will not be used, the formulation is kept general for shunted RL series circuits.

In this layerwise model, it is assumed that the origin of the  $z$ -axis is the medium plane of the core layer, no slip occurs at the interfaces between layers, the displacements are continuous along the interfaces, and the viscoelastic core, ( $v$ ), has transverse compressibility.

The composite layers and piezoelectric patches are modeled with first-order shear deformation theory (FSDT) and the viscoelastic core with a higher-order shear deformation theory (HSDT). The displacement fields for each layer with its respective degrees of freedom can be found in [19].

All the materials used in each layer are linear, orthotropic, and homogeneous. The viscoelastic core material properties are also complex and frequency dependent.

In this application, it is considered that all the layers in the sandwich plate model are constituted by orthotropic materials. However, as the viscoelastic core displacement is modeled differently from the composite laminate and the piezoelectric layers, the constitutive relations are different for both.

For the laminated composite and piezoelectric layers, it is assumed zero transverse normal stress, with the constitutive relations being described as [20]:

$$\begin{Bmatrix} \sigma_{11} \\ \sigma_{22} \\ \tau_{23} \\ \tau_{13} \\ \tau_{12} \end{Bmatrix} = \begin{bmatrix} Q_{11} & Q_{12} & 0 & 0 & 0 \\ Q_{12} & Q_{22} & 0 & 0 & 0 \\ 0 & 0 & Q_{44} & 0 & 0 \\ 0 & 0 & 0 & Q_{55} & 0 \\ 0 & 0 & 0 & 0 & Q_{66} \end{bmatrix}^E \begin{Bmatrix} \varepsilon_{11} \\ \varepsilon_{22} \\ \gamma_{23} \\ \gamma_{13} \\ \gamma_{12} \end{Bmatrix} + \begin{bmatrix} 0 & 0 & e_{31}^* \\ 0 & 0 & e_{32}^* \\ 0 & e_{24} & 0 \\ e_{15} & 0 & 0 \\ 0 & 0 & 0 \end{bmatrix} \begin{Bmatrix} E_{f1} \\ E_{f3} \\ E_{f3} \end{Bmatrix}, \quad (1)$$

$$\begin{Bmatrix} D_1 \\ D_2 \\ D_3 \end{Bmatrix} = \begin{bmatrix} 0 & 0 & 0 & e_{15} & 0 \\ 0 & 0 & e_{24} & 0 & 0 \\ e_{31}^* & e_{31}^* & 0 & 0 & 0 \end{bmatrix} \begin{Bmatrix} \varepsilon_{11} \\ \varepsilon_{22} \\ \gamma_{23} \\ \gamma_{13} \\ \gamma_{12} \end{Bmatrix} + \begin{bmatrix} \epsilon_{11} & 0 & 0 \\ 0 & \epsilon_{22} & 0 \\ 0 & 0 & \epsilon_{33}^* \end{bmatrix}^e \begin{Bmatrix} E_{f1} \\ E_{f3} \\ E_{f3} \end{Bmatrix}$$

where  $\sigma_{ii}$  and  $\tau_{ij}$  are the normal and shear stress components, respectively,  $\varepsilon_{ii}$  and  $\gamma_{ij}$  are the strain components,  $E_{fi}$  is the electric field,  $D_i$  is the electric displacement field,  $Q_{ij}^E$  are the reduced stiffness coefficients at constant electric field,  $e_{ij}$  and  $e_{ij}^*$  are the electromechanical and reduced electromechanical coupling coefficients (piezoelectric effect), respectively, and  $\epsilon_{ii}$  and  $\epsilon_{33}^*$  are the dielectric and reduced dielectric constants, measured at constant strain. The equations to compute the reduced values can be found in [20].

The set of equations (1) is easily applied to the laminated composite layers since it is only needed that their electromechanical coupling coefficients vanish.

For the viscoelastic core, a full 3D orthotropic model is considered [21]:

$$\begin{Bmatrix} \sigma_{11} \\ \sigma_{22} \\ \sigma_{33} \\ \tau_{23} \\ \tau_{13} \\ \tau_{12} \end{Bmatrix} = \begin{bmatrix} C_{11} & C_{12} & C_{13} & 0 & 0 & 0 \\ C_{12} & C_{22} & C_{23} & 0 & 0 & 0 \\ C_{13} & C_{23} & C_{33} & 0 & 0 & 0 \\ 0 & 0 & 0 & C_{44} & 0 & 0 \\ 0 & 0 & 0 & 0 & C_{55} & 0 \\ 0 & 0 & 0 & 0 & 0 & C_{66} \end{bmatrix}^E \begin{Bmatrix} \varepsilon_{11} \\ \varepsilon_{22} \\ \varepsilon_{33} \\ \gamma_{23} \\ \gamma_{13} \\ \gamma_{12} \end{Bmatrix} \quad (2)$$

where  $C_{ij}$  are the stiffness coefficients, in terms of engineering quantities, whose expressions are found in [21]. In the context of this work, the stiffness coefficients of the viscoelastic layer are complex and frequency dependent, with the complex modulus being obtained as a consequence of using the elastic-viscoelastic correspondence principle [22]. Thus, for an isotropic viscoelastic material with constant Poisson's ratio, the shear modulus is complex and frequency dependent:

$$G(j\omega) = G'(\omega) (1 + j\eta_G(\omega)) \quad (3)$$

where  $G'$  is the storage shear modulus,  $\eta_G$  is the associated material loss factor, and  $j = \sqrt{-1}$  is the imaginary unit.

The finite element formulation uses 8-node serendipity elements with 17 mechanical degrees of freedom per node and one electrical degree of freedom per piezoelectric layer. The finite element formulation leads to the following equilibrium equation in the frequency domain [15]:

$$[\mathbf{K}^*(\omega) - \omega^2 \mathbf{M}_{\mathbf{uu}}] \mathbf{U}(\omega) = \mathbf{F}(\omega) \quad (4)$$

where  $\mathbf{M}_{\mathbf{uu}}$  is the mass matrix,  $\mathbf{U}(\omega)$  is the vector of amplitudes of displacement,  $\mathbf{F}(\omega) = \mathcal{F}(F_i(t))$  is the Fourier transform of the time domain force history  $F_i(t)$ , and  $\mathbf{K}^*$  is the condensed stiffness matrix given by:

$$\mathbf{K}^*(\omega) = \mathbf{K}_{\mathbf{uu}}(\omega) - \mathbf{K}_{\mathbf{u}\phi} \mathbf{Z}_e(\omega) [\mathbf{I} + \mathbf{K}_{\phi\phi} \mathbf{Z}_e(\omega)]^{-1} \mathbf{K}_{\mathbf{u}\phi}^T \quad (5)$$

where  $\mathbf{K}_{\mathbf{uu}}(\omega)$  is the complex stiffness matrix,  $\mathbf{K}_{\mathbf{u}\phi}$  is the electromechanical coupling stiffness matrix,  $\mathbf{K}_{\phi\phi}$  is the dielectric stiffness matrix,  $\mathbf{I}$  is the identity matrix, and  $\mathbf{Z}_{\mathbf{e}}(\omega)$  is the electrical impedance matrix of the RL shunts, given by:

$$\mathbf{Z}_{\mathbf{e}} = \begin{bmatrix} j\omega R_1 - \omega^2 L_1 & \cdots & 0 & \cdots & 0 \\ 0 & j\omega R_2 - \omega^2 L_2 & \cdots & \cdots & 0 \\ \vdots & \ddots & \vdots & \ddots & \vdots \\ 0 & \cdots & \cdots & j\omega R_{np} - \omega^2 L_{np} & \cdots \end{bmatrix} \quad (6)$$

where  $R_i$  and  $L_i$  are the electrical resistance and inductance of the piezoelectric layer  $i$ , and  $j$  is the imaginary unit.

The finite element problem is solved in two steps: First, the following eigenvalue problem given by the nonlinear equation is solved in order to obtain the natural frequencies of the plate for a specific patch distribution [19]:

$$[\mathbf{K}^*(\omega) - \lambda_n^* \mathbf{M}_{\mathbf{uu}}] \mathbf{U}_n = 0 \quad (7)$$

where  $\lambda_n^*$  is the complex eigenvalue given by

$$\lambda_n^* = \lambda_n (1 + j\eta_n) \quad (8)$$

where  $\lambda_n = \omega_n^2$  is the real part of the complex eigenvalue and  $\eta_n$  is the correspondent modal loss factor.

The nonlinear eigenvalue problem is solved iteratively using the Fortran library ARPACK [23] with a shift-invert transformation. The iterative process ends when the stopping criteria are met,

$$\frac{\|\omega_i - \omega_{i-1}\|}{\omega_{i-1}} \leq \epsilon, \quad (9)$$

where  $\omega_i$  and  $\omega_{i-1}$  are the current and previous iteration real parts of the complex eigenvalue for the current mode, respectively, and  $\epsilon$  is the user-defined convergence tolerance.

Finally, the forced vibration problem is solved in the obtained frequencies in order to obtain the plate response in each peak by Eq. (4) with  $\omega = \omega_n$ .

### 3 Acoustic response

The plate is surrounded by a light fluid (air) to which it radiates noise. Since the mass of the fluid can be neglected, the acoustic and structural problems can be solved separately: First the structural problem is solved, and then the noise radiated by the plate into the surrounding medium is obtained and used as an indicator of its performance. As such, the acoustic indicator chosen for the present work is the RSP ( $\Pi$ ), which can be obtained from Rayleigh's integral.

Using the elementary radiators approach, we avoid having to solve the Rayleigh integral, and the RSP can be computed as [15]:

$$\Pi = \mathbf{v}_n^H \mathbf{R} \mathbf{v}_n \quad (10)$$

where  $\mathbf{v}_n$  is the vector with the amplitude of the normal velocity of each element (obtained as a solution of the finite element problem),  $H$  is the Hermitian transpose, and  $\mathbf{R}$  is the radiation resistance matrix for the elementary radiators given by:

$$\mathbf{R} = \frac{\omega^2 \rho_0 S_e^2}{4\pi c_0} \begin{bmatrix} 1 & \frac{\sin(kr_{12})}{kr_{12}} & \cdots & \frac{\sin(kr_{1R})}{kr_{1R}} \\ \frac{\sin(kr_{21})}{kr_{21}} & 1 & \cdots & \frac{\sin(kr_{2R})}{kr_{2R}} \\ \vdots & \vdots & \ddots & \vdots \\ \frac{\sin(kr_{R1})}{kr_{R1}} & \frac{\sin(kr_{R2})}{kr_{R2}} & \cdots & 1 \end{bmatrix} \quad (11)$$

where  $\rho_0$  is the mass density of the surrounding fluid,  $c_0$  is the speed of sound in the fluid,  $k = \omega/c_0$  is the wave number,  $S_e$  is the surface area of each element, and  $r_{ij}$  is the distance between the center of the elements  $i$  and  $j$ .

**Table 1** Material properties of the carbon plies

$E_1$ [GPa]	$E_2$ [GPa]	$G_{12}$ [GPa]	$G_{13}$ [GPa]	$G_{23}$ [GPa]	$\nu_{12}$	$\rho$ [kg/m <sup>3</sup> ]
130.8	10.6	5.6	4.2	3.0	0.36	1543

**Table 2** Reduced material properties for PZT-4 [20,26]

$E$ [GPa]	$G$ [GPa]	$\nu_{12}$	$e^*$ [N/V · m]	$\epsilon^*$ [F/m]	$\rho$ [kg/m <sup>3</sup> ]
$E_1 = 81.3$ $E_2 = 81.3$	$G_{12} = 30.6$ $G_{13} = 25.6$ $G_{23} = 25.6$	$\nu_{12} = 0.33$	$e_{31}^* = -14.9$ $e_{32}^* = -14.9$	$\epsilon_{33}^* = 4.24 \times 10^{-9}$	$\rho = 7500$

**Table 3** Natural frequencies and respective frequency response for the first 5 modes of the plate

Mode	Frequency [Hz]	$\Pi$ [W]
1	179.829	$4.110 \times 10^6$
2	309.377	0.478
3	387.113	1.773
4	501.101	$8.772 \times 10^4$
5	560.982	$7.024 \times 10^3$

Further details on this approach can be found in [24].

This method can be applied to any plane surface in an infinite baffle for any given boundary conditions, as it only requires the knowledge of the surface geometry, the properties of the fluid, and the normal velocity field distribution.

#### 4 Problem statement

We consider a  $200 \times 300$  mm<sup>2</sup> laminated sandwich plate made of carbon fiber plies with a viscoelastic core and with all edges clamped. The stacking sequence for the carbon fiber plies is  $[0^\circ/90^\circ/+45^\circ]$  and  $[+45^\circ/90^\circ/0^\circ]$  for  $e_1$  and  $e_2$ , respectively, making the total stacking symmetric when patch-free. Each carbon ply is 0.5 mm thick (totaling up to 1.5 mm for each  $e_1$  and  $e_2$ ), and the viscoelastic core is 2.5 mm thick. The carbon plies are orthotropic, whose material properties can be found in Table 1.

The viscoelastic core is made of an isotropic polymer with  $\nu = 0.49$ ,  $\rho = 1300$  kg/m<sup>3</sup>, and a complex shear modulus, described by a five-parameter fractional derivative model [25]. The complex shear modulus is obtained as:

$$G(j\omega) = G_0 + G_0(d-1) \frac{(j\omega\tau)^\alpha}{1 + (j\omega\tau)^\beta} \quad (12)$$

where  $G_0 = 0.8$  MPa is the static shear modulus,  $d = 1.05$ ,  $\alpha = 0.566$ ,  $\beta = 0.558$ , and  $\tau = 7.23 \times 10^{-10}$  s is the relaxation time. Since the goal of this paper is to evaluate the damping effect of shunted circuits in piezoelectric patches, it is important that the damping effect of the viscoelastic core is minimal; hence, we use  $d = 1.05$ . We do not eliminate completely the damping of the viscoelastic core ( $d = 1$ ) in order to prevent the response amplitudes for the undamped configurations from tending to infinity.

Piezoelectric patches are bonded to the upper surface of the plate. Both have top and bottom surfaces electroded, which ensure the voltage is constant along each surface. The patch dimensions are  $33.3 \times 50$  mm<sup>2</sup> ( $\frac{1}{36}$  of the total area of the plate), and each one is 0.9 mm thick, with its material being lead zirconate titanate (PZT-4) whose reduced properties can be found in Table 2.

Figure 2 shows the modal vertical deformation of the plate for the first five modes. Table 3 shows the correspondent natural frequencies and the respective RSP when a 100 Pa incident wave is applied to the bottom surface of the plate at  $t = 0$  s. This same load is the one applied in the optimization problem.

The goal of this study is to obtain the optimal configurations that minimize weight, equipotential zones, and sound radiation, for the first five vibration modes. This defines a multiobjective optimization problem

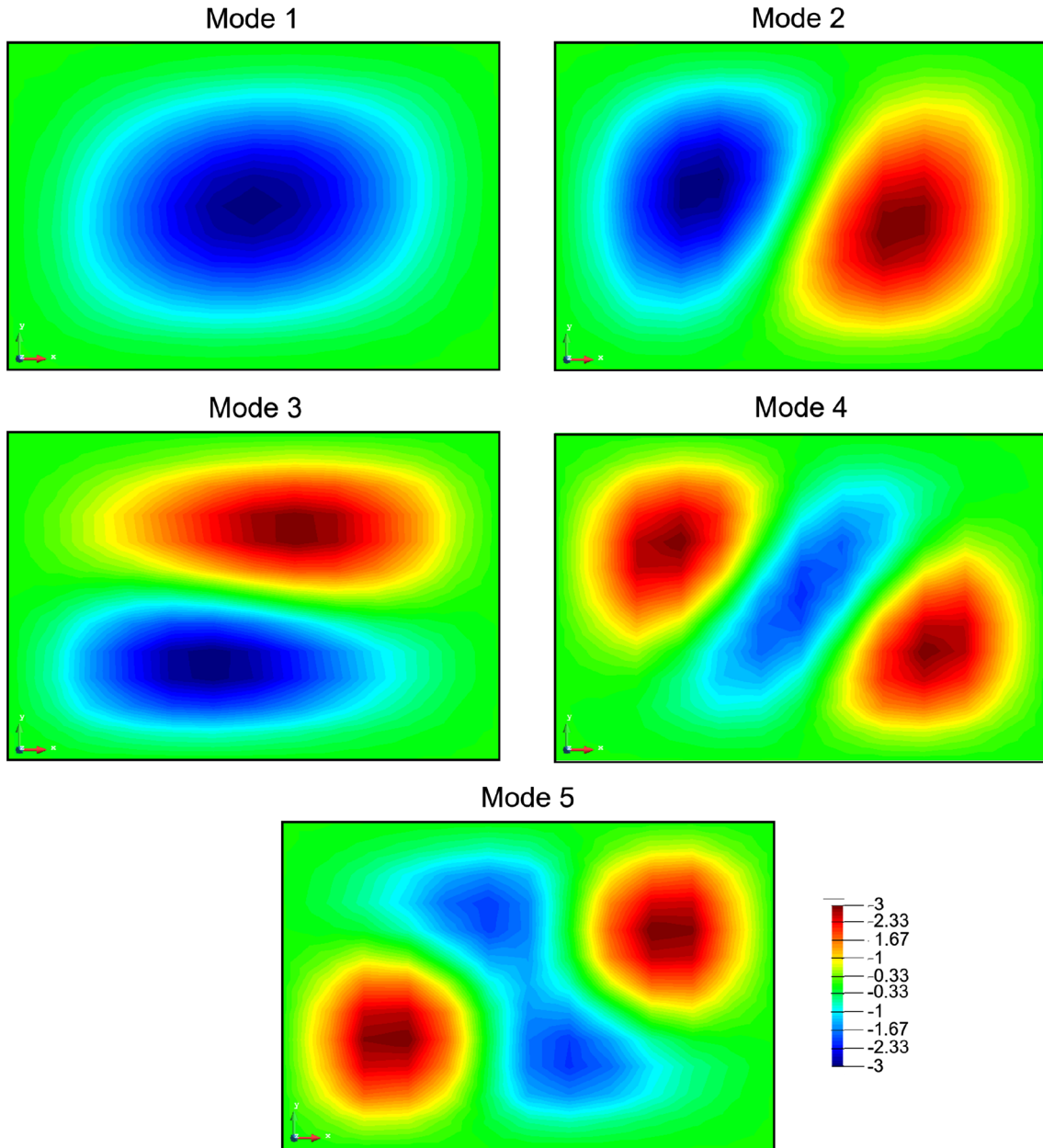


**Fig. 2** Plate response for the first five modes

with seven objectives. The first of the three objectives is to minimize the total added mass of the patches  $f_1 = \sum_i m_i$ . The second is to minimize the number of equi-potential zones  $f_2$  at the surface of the plate. The remaining 5 objectives,  $f_3$ – $f_7$ , are to minimize the RSP for modes 1–5, respectively, defined by equation (10). The multi-objective optimization problem is defined as:

$$\begin{aligned}
 \min_x \quad & F(x) = (f_1(x), f_2(x), f_3(x), f_4(x), f_5(x), f_6(x), f_7(x))^T \\
 \text{s. t.} \quad & x_i \in [0, 1], \quad i = 1, \dots, 9 \\
 & x_j \in [0 : 100 : 15000] \Omega, \quad j = 1, \dots, 13
 \end{aligned} \tag{13}$$

where  $x_i$  is a real design variable that denotes whether or not there is a patch on position  $i$  (if  $x_i < 0.5$  is rounded to 0, meaning there is no patch, and rounded to 1 otherwise) and  $x_j$  is a design variable that has the resistance value of the shunt circuit of the equipotential zone  $j$ .

1	2	3	3	2	1
4	5	6	6	5	4
7	8	9	9	8	7
7	8	9	9	8	7
4	5	6	6	5	4
1	2	3	3	2	1

**Fig. 3** Patch distribution in the full plate when considering only a quarter of it

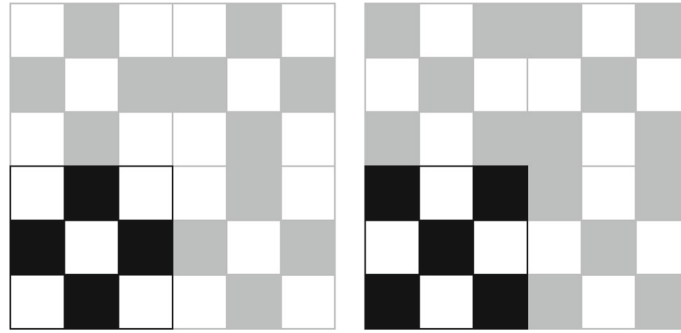


**Fig. 4** Initial solutions for the multi-objective problem (14)

The plate is discretized into a  $6 \times 6$  mesh with a total of 36 elements. In order to reduce the computational effort, only a quarter of the plate is considered, with the patches being added symmetrically across the plate (Fig. 3). It is important to note that the multi-objective optimization problem defined in (13) already contemplates these assumptions.

In order to improve convergence and keep the computation times at reasonable values, it was decided to start by obtaining the optimal configurations for each one of the first five vibration modes, independently. To do this, we start by solving the five problems presented in (14), with only three objectives (mass, equipotential zones, and the RSP for the targeted mode  $k = 1, \dots, 5$ ), keeping the same design variables as in problem (13),

$$\begin{aligned}
 \min_x \quad & F(x) = (f_1(x), f_2(x), f_k(x))^T \\
 \text{s. t.} \quad & x_i \in [0, 1], \quad i = 1, \dots, 9 \\
 & x_j \in [0 : 100 : 15000] \Omega, \quad j = 1, \dots, 13.
 \end{aligned} \tag{14}$$

The solutions obtained for these five optimizations are then serving to initialize the problem with seven variables defined in (13).

The optimization problems are solved using DMS [16]. The optimization problems defined in (14) were initialized considering the worst case scenarios for objective  $f_2$  and with R shunts set to 0, maximizing the RSP for each mode (objectives  $f_3$ – $f_7$ ), whose configurations are presented in Fig. 4.

## 5 Results

We present in this Section some of the results obtained in the different multi-objective optimization problems. First, the results of the five problems with 3 objectives (14) are presented, with each problem (14) commented individually:

- For the first mode ( $k = 3$ ), 4 non-dominated solutions were obtained. Figure 5 displays these solutions on the planes  $f_1$ – $f_3$  and  $f_2$ – $f_3$  alongside their respective resistances. Each configuration was able to reduce the sound levels of the first mode in at least seven orders of magnitude (from Table 3,  $\Pi = 4.11 \times 10^6$  W), with the solutions 3 and 4 reducing up to nine orders of magnitude, up to  $\sim 10^{-2}$  W. One observation that

can be made is that the objectives  $f_2$  and  $f_3$  are not conflicting, since there is only one zone with relevant strain that occurs in the middle of the panel, meaning patches should only be placed there.

- For the second mode ( $k = 4$ ), 16 non-dominated solutions were obtained. Figure 6 displays these solutions on the planes  $f_1-f_4$  and  $f_2-f_4$  alongside their respective resistances (when there is more than one equipotential zone, the resistance values are ordered from left to right, from bottom to top, which remains true for the remaining Tables shown throughout the remaining of the work). The configurations obtained were able to reduce the sound levels from  $4.78 \times 10^{-1}$  W (Table 3) to  $10^{-4} \sim 10^{-5}$  W. Two key observations can be made. The first is the occurrence of saturation of the resistances in the maximum value in some of the solutions obtained, meaning a higher damping effect could be attained if the resistance range was increased. The other one is the existence of equipotential zones with no resistance. For some patches, this happens due to the symmetry condition imposed, as placing them in a position forces the placement in other places that would not need them. In other cases, however, the equipotential zone in the centre of the plate is the one with no resistance (where the patches placed due to symmetry are adjacent). This could happen due to the fact that the patches, even in short-circuit boundary conditions, still increase the mass and the stiffness, slightly changing the response, thus improving the acoustic performance (this effect is showcased in the article [15], where the responses of the patch-free plate and of a chosen configuration in short circuit are compared).
- For the third mode ( $k = 5$ ), 16 non-dominated solutions were obtained. Figure 7 displays these solutions on the planes  $f_1-f_5$  and  $f_2-f_5$  alongside their respective resistances. The configurations obtained were able to reduce the sound levels from 1.773 W (Table 3) to  $10^{-4} \sim 10^{-6}$  W. The saturation of resistances was again noticed. The same phenomena from the previous mode happened, where the patches in the middle did not have a resistance, thus reducing the acoustic levels due to change in mass/stiffness.
- For the fourth mode ( $k = 6$ ), 3 non-dominated solutions were obtained. Figure 8 displays these solutions on the planes  $f_1-f_6$  and  $f_2-f_6$  alongside their respective resistances. The acoustic levels were reduced from  $8.772 \times 10^4$  W (Table 3) to  $\sim 10^{-2}$  W.
- For the fifth mode ( $k = 7$ ), 14 non-dominated solutions were obtained. Figure 9 displays these solutions on the planes  $f_1-f_7$  and  $f_2-f_7$  alongside their respective resistances. The configurations obtained were able to reduce the RSP from  $7.024 \times 10^3$  W to  $10^{-4} \sim 10^{-5}$  W. It was again noticed that some solutions had saturated resistances. Solutions 6 and 9 had again patches with no resistances, similar to modes 2 ( $k = 4$ ) and 3 ( $k = 5$ ).

Overall, each problem was able to generate solutions that effectively reduce the RSP for its targeted mode. The results also suggest that patches should be placed where there is more relevant strain.

The multi-objective problem with 7 objectives (13) was initialized with a total of 53 solutions, which correspond to the set of all solutions obtained in five problems (14) previously solved. The optimization result obtained for problem (13) was a set with 1793 non-dominated solutions after a total of 10048 evaluations of the objective function (in each of the evaluations of the objective function the value of the seven objectives is calculated). It is important to note that the algorithm employs a cache that stores the value of the objective functions of every evaluated solution until the current evaluation, meaning that if in a new iteration a previous analyzed solution is considered, the values of the objective function do not need to be computed, thus reducing the computational efforts. Since the goal in this work is to obtain the best solution that can reduce the overall levels for several modes, it is important to compare the responses of the different modes equally. As such, the response for each mode has been normalized by Eq. 15, with the solutions being then compared by the norm of  $L_1$  (16), [27]. That is, norm of  $L_1$  is used to classify the solutions obtained in relation to the modes (the smallest value of the norm of  $L_1$  corresponds to the best solution for the first five modes simultaneously),

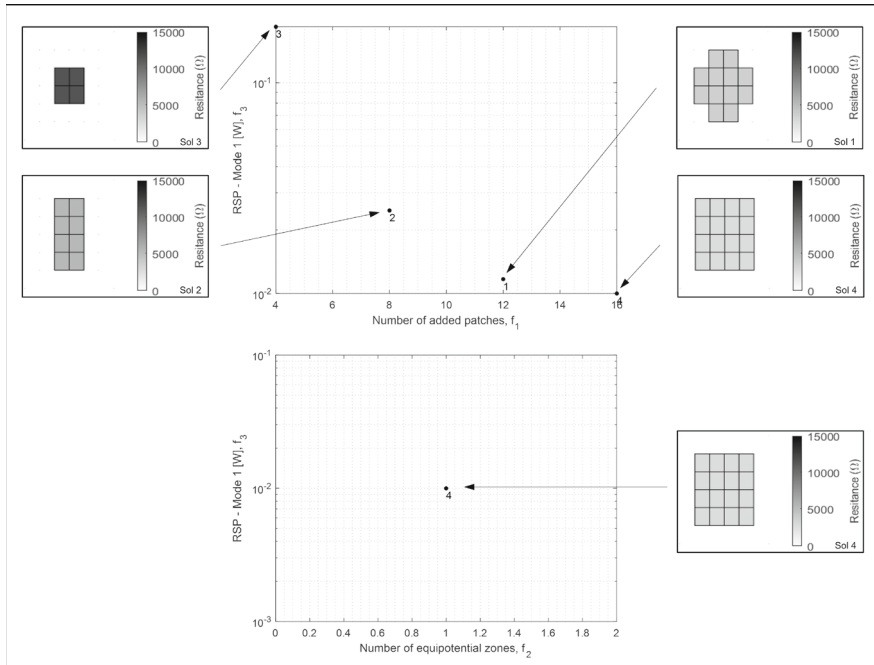
$$\bar{A} = \frac{A_{k,i} - \min_i A_{k,i}}{\max_i A_{k,i} - \min_i A_{k,i}}, \quad (15)$$

$$L_1 = \min \left( \sum_{k=3}^7 \bar{A}_{k,1}, \sum_{k=3}^7 \bar{A}_{k,2}, \dots, \sum_{k=3}^7 \bar{A}_{k,j} \right), \quad (16)$$

where in Eqs. (15) and (16)  $A$  is the matrix of non-dominated solutions,  $k = 3, \dots, 7$  are the objective functions,  $i$  is the number of the non-dominated solution, and  $j$  is the number of non-dominated solutions.

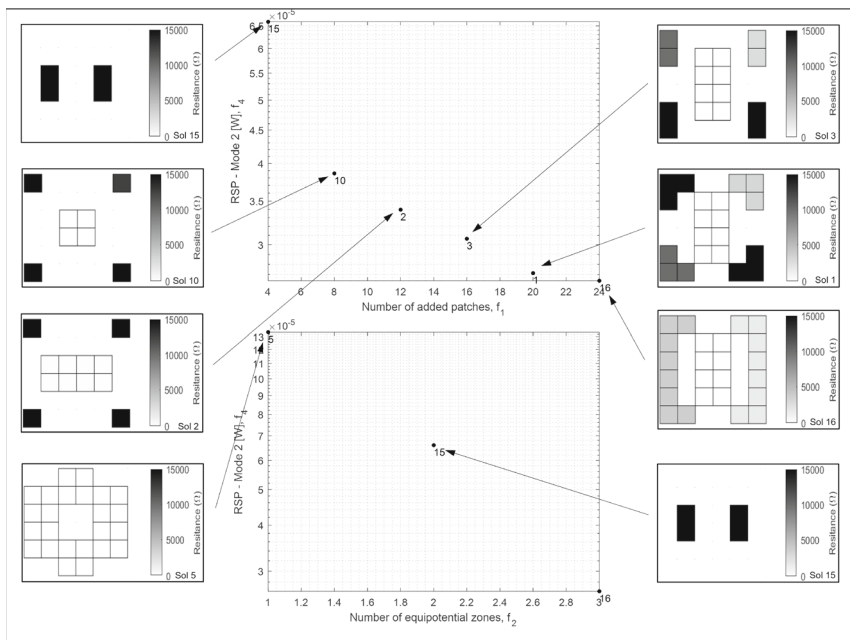
Figure 10 presents the best solutions, within the 1793 non-dominated solutions, obtained after solving problem (13) alongside their resistances, for the objectives  $f_1$  and  $f_2$  and for the norm of  $L_1$ . Table 4 shows the values of each objective function displayed in Fig. 10.





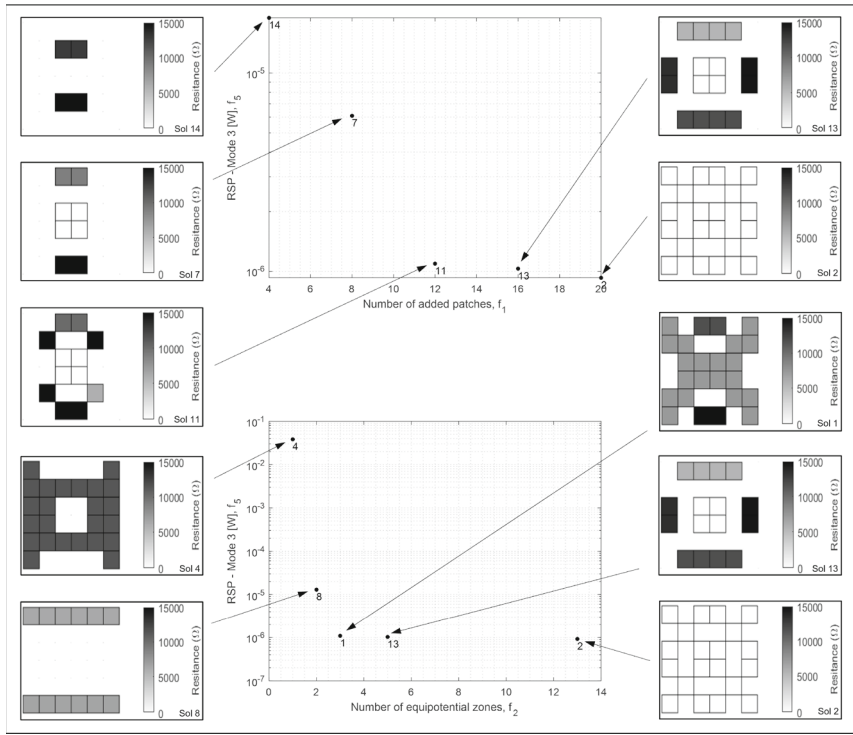
Solution	R ( $\Omega$ )
1	3600
2	5400
3	11500
4	2700

**Fig. 5** Non-dominated solutions in respect of damping versus the added mass ( $f_1$ ) and versus the number of equipotential zones ( $f_2$ ) for mode 1 ( $f_3$ ) alongside their respective resistances



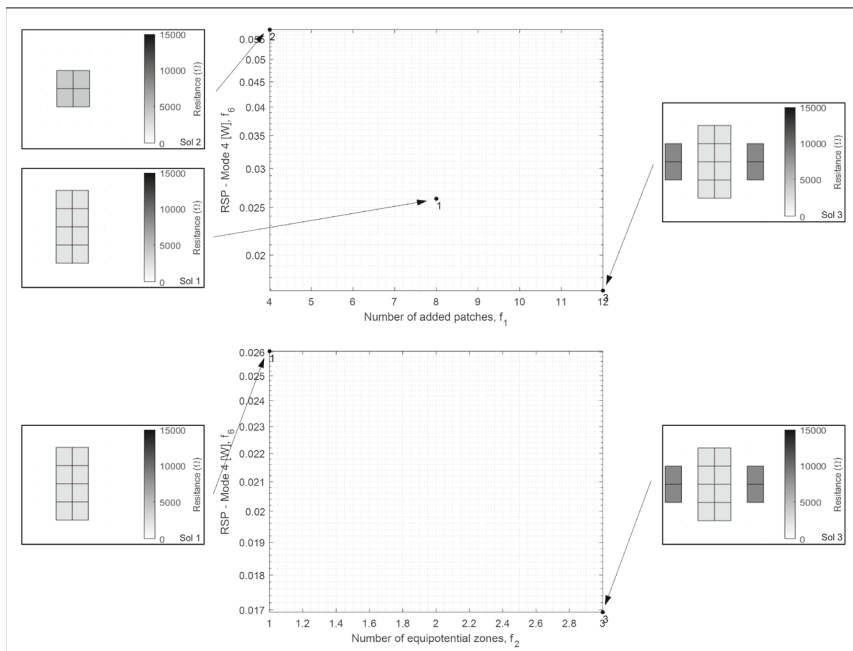
Solution	R ( $\Omega$ )
1	10100
	15000
	0
	15000
2	3200
	15000
	15000
	100
	15000
3	15000
	15000
	0
	10000
	2700
10	15000
	15000
	0
	15000
15	12600
	15000
16	3700
	1500

**Fig. 6** Non-dominated solutions in respect of damping versus the added mass ( $f_1$ ) and versus the number of equipotential zones ( $f_2$ ) for mode 2 ( $f_4$ ) alongside their respective resistances



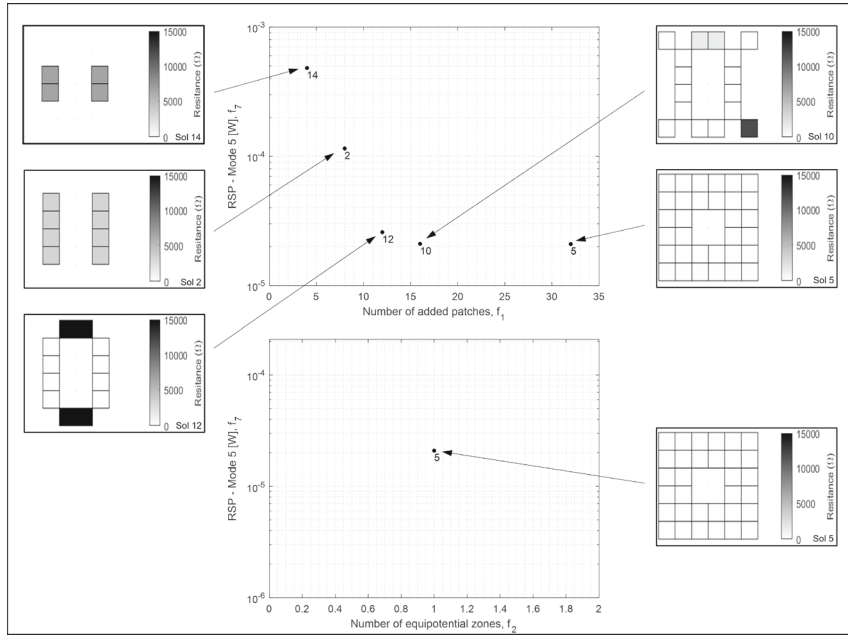
Solution	R ( $\Omega$ )
1	7400
	15000
	11800
2	0
4	11400
7	15000
	0
8	9100
	6700
	6400
11	15000
	15000
	6000
	0
	15000
	15000
	10300
13	11800
	13600
	0
	14800
	5600
14	11400
	15000

**Fig. 7** Non-dominated solutions in respect of damping versus the added mass ( $f_1$ ) and versus the number of equipotential zones ( $f_2$ ) for mode 3 ( $f_5$ ) alongside their respective resistances



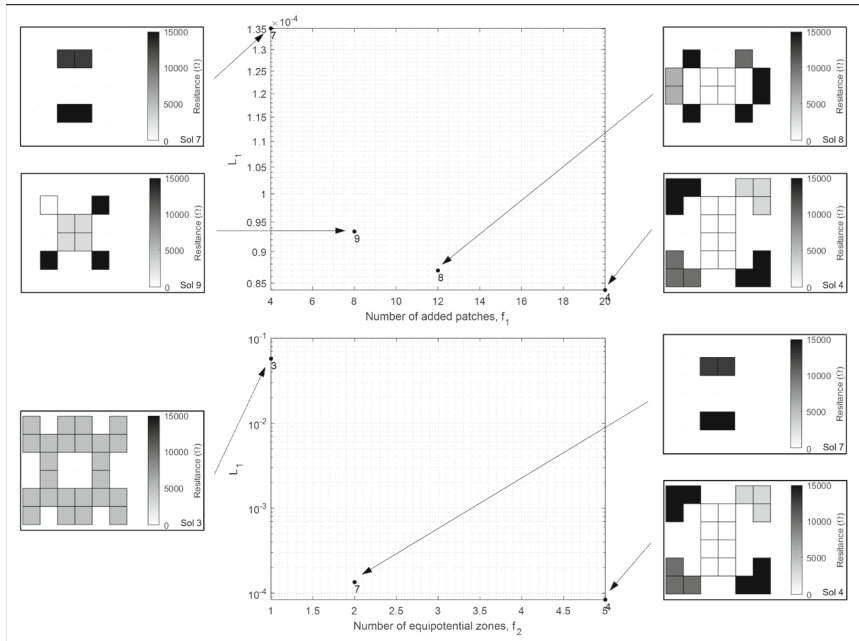
Solution	R ( $\Omega$ )
1	2200
2	4100
3	2200
	8600
	8600

**Fig. 8** Non-dominated solutions in respect of damping versus the added mass ( $f_1$ ) and versus the number of equipotential zones ( $f_2$ ) for mode 4 ( $f_6$ ) alongside their respective resistances



Solution	R ( $\Omega$ )
4	3300
5	200
10	0
	12000
	0
	0
	1500
	0
12	15000
	0
	0
14	15000
	6700
	6700

**Fig. 9** Non-dominated solutions in respect of damping versus the added mass ( $f_1$ ) and versus the number of equipotential zones ( $f_2$ ) for mode 5 ( $f_7$ ) alongside their respective resistances



Solution	R ( $\Omega$ )
3	4800
4	10100
	15000
	0
	15000
7	3200
	15000
8	12900
	15000
	6000
	0
	15000
	15000
9	10300
	15000
	15000
	2800
	0
	15000

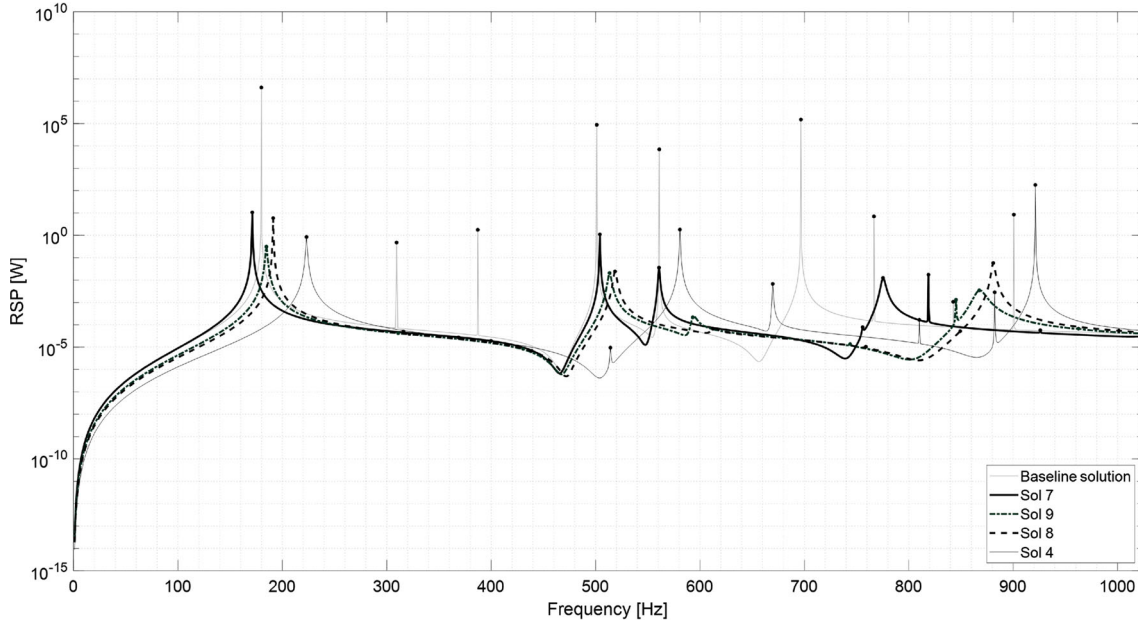
**Fig. 10** Non-dominated solutions obtained in problem (13) in respect of the norm  $L_1$  versus the added mass ( $f_1$ ) and versus the number of equipotential zones ( $f_2$ ) alongside their respective resistances

From Table 4, we notice that for modes 2 to 5 ( $f_4$ – $f_7$ ) the solutions picked were able to reduce the sound levels similarly to the solutions obtained in five problems (14). The same did not happen for the first mode, as it was previously reduced up to  $10^{-2}$  W. Still, these solutions are able to reduce the first mode from  $\Pi = 4.11 \times 10^6$  W to  $10^0 \sim 10^{-2}$  W while still reducing the noise in the remaining modes.

From the solutions displayed in Fig. 10, the RSP curves were calculated in the frequency range 0–1024 Hz, being displayed in Figs. 11 and 12. In these Figures, it is seen that for every solution (apart from solution 7), it was possible to reduce the RSP across the different modes of the panel. It is important to note that the values

**Table 4** Values of the components of the objective function defined in (13) for the solutions displayed in Fig. 10

Sol no.	$f_1$	$f_2$	$f_3$ [W]	$f_4$ [W]	$f_5$ [W]	$f_6$ [W]	$f_7$ [W]
3	24	1	$2.121 \times 10^{+2}$	$1.116 \times 10^{-2}$	$5.957 \times 10^{-2}$	$2.254 \times 10^{-1}$	3.342
4	20	1	$8.484 \times 10^{-1}$	$2.714 \times 10^{-5}$	$9.465 \times 10^{-6}$	1.817	$6.766 \times 10^{-3}$
7	4	2	$1.065 \times 10^{+1}$	$4.980 \times 10^{-5}$	$1.901 \times 10^{-5}$	1.104	$3.595 \times 10^{-2}$
8	12	7	5.912	$3.894 \times 10^{-5}$	$6.855 \times 10^{-6}$	$2.432 \times 10^{-2}$	$6.688 \times 10^{-5}$
9	8	5	$3.109 \times 10^{-1}$	$4.226 \times 10^{-5}$	$8.351 \times 10^{-6}$	$2.085 \times 10^{-2}$	$2.156 \times 10^{-4}$

**Fig. 11** RSP curves for the non-dominated solutions displayed in the plane  $f_1-L_1$ 

of many resistances of these solution have saturated, meaning a higher damping effect should be obtained by increasing the considered range.

Additionally, a multi-objective optimization problem was also defined, in order to improve the solutions obtained in (13). This problem is defined in Eq. (17) and considers the norm  $L_1$  as an objective, while keeping the first two. Problem (17) was started from the non-dominated solutions obtained in (13),

$$\begin{aligned}
 \min \quad & F(x) = (f_1(x), f_2(x), L_1(x))^T \\
 \text{s. t.} \quad & x_i \in [0, 1], \quad i = 1, \dots, 9 \\
 & x_j \in [0 : 100 : 15000] \Omega, \quad j = 1, \dots, 13.
 \end{aligned} \tag{17}$$

A total of 11 non-dominated solutions were obtained, with some of them displayed in Fig. 13 in the planes  $f_1 - L_1$  and  $f_2 - L_1$ , besides their respective resistances. Table 5 shows the values of each objective function from problem (17) of the solutions displayed in Fig. 13. Table 6 displays the RSP for these solutions in each of the first five modes.

When comparing the RSP from the solutions obtained in problem (17), displayed in Table 6, with the solutions obtained in problem (13), shown in Table 4, we notice a significant improvement in the first, fourth, and fifth modes, without affecting the remaining two.

The two configurations 8 and 4 from Fig. 10 and the two configurations 11 and 7 from Fig. 13 were chosen in order to compare both RSP curves, where the first two have the same  $f_1$  and the last two have the same configuration with different resistances. Figures 14 and 15 show the RSP curves for these points, respectively. In both cases, the solutions obtained by solving problem (17) had lower responses for the first five modes than the ones obtained in problem (13), meaning that this approach is capable of generating solutions that can reduce the overall response of the plate for the first five modes.

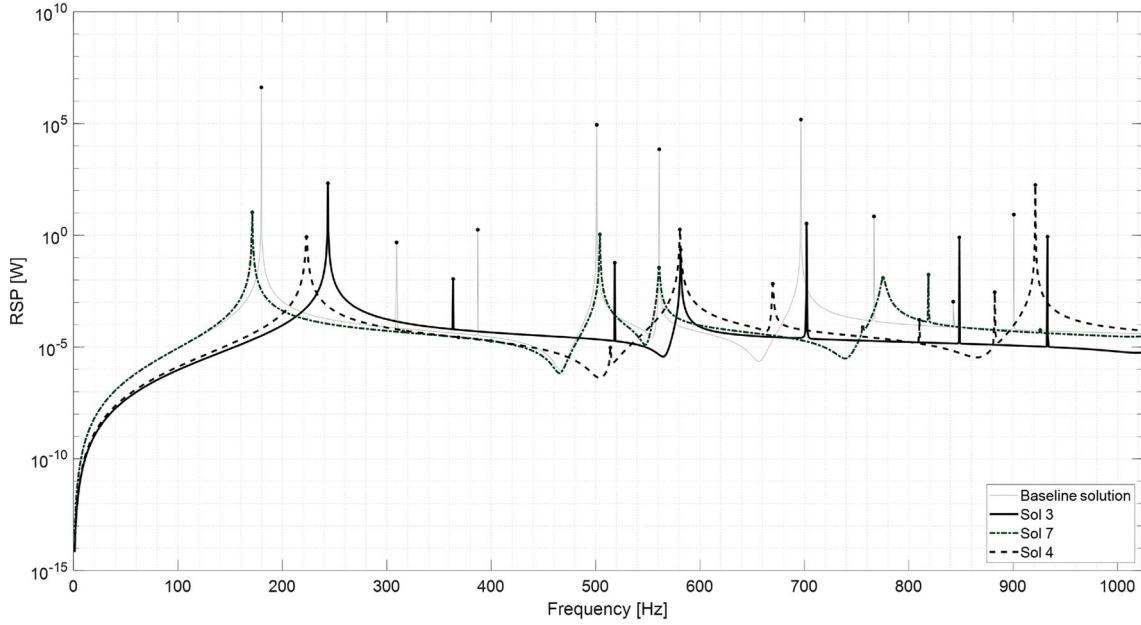


Fig. 12 RSP curves for the non-dominated solutions displayed in the plane  $f_2-L_1$

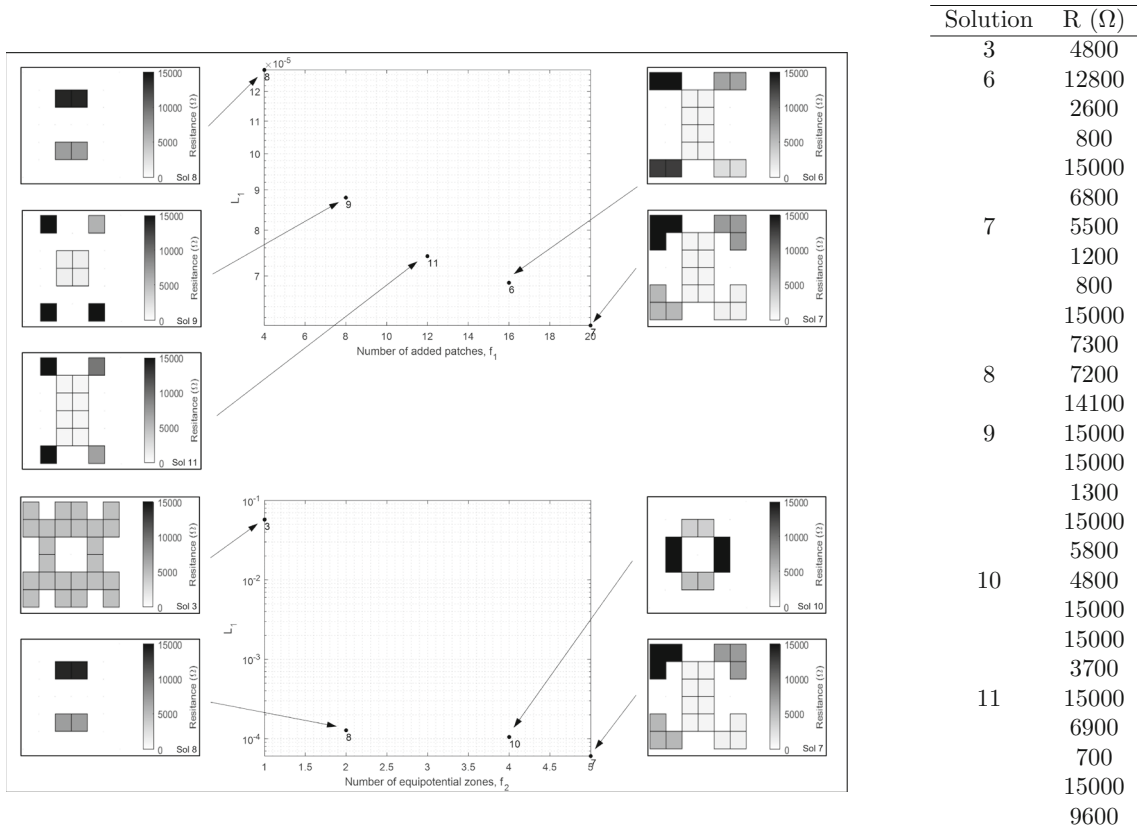


Fig. 13 Non-dominated solutions obtained in problem (17) in respect of the norm  $L_1$  versus the added mass ( $f_1$ ) and versus the number of equipotential zones ( $f_2$ ) alongside their respective resistances

**Table 5** Values of the components of the objective function defined in (17) for the solutions displayed in Fig. 13

Sol no.	$f_1$	$f_2$	$L_1$
3	24	1	$5.746 \times 10^{-2}$
6	16	5	$6.861 \times 10^{-5}$
7	20	5	$6.057 \times 10^{-5}$
8	4	2	$1.278 \times 10^{-4}$
9	8	5	$8.798 \times 10^{-5}$
10	8	4	$1.052 \times 10^{-4}$
11	12	5	$7.416 \times 10^{-5}$

**Table 6** RSP for the solutions of problem (17) displayed in Fig. 13

Sol no.	Mode 1 [W]	Mode 2 [W]	Mode 3 [W]	Mode 4 [W]	Mode 5 [W]
3	$2.121 \times 10^2$	$1.116 \times 10^{-2}$	$5.957 \times 10^{-2}$	$2.254 \times 10^{-1}$	3.342
6	$1.457 \times 10^{-1}$	$3.125 \times 10^{-5}$	$4.811 \times 10^{-6}$	$3.949 \times 10^{-2}$	$7.360 \times 10^{-4}$
7	$1.226 \times 10^{-1}$	$2.759 \times 10^{-5}$	$3.881 \times 10^{-6}$	$4.056 \times 10^{-2}$	$1.555 \times 10^{-3}$
8	$1.578 \times 10^{+1}$	$4.678 \times 10^{-5}$	$1.934 \times 10^{-5}$	$9.776 \times 10^{-1}$	$2.884 \times 10^{-2}$
9	$4.390 \times 10^{-1}$	$3.903 \times 10^{-5}$	$9.562 \times 10^{-6}$	$6.476 \times 10^{-2}$	$1.230 \times 10^{-3}$
10	$2.139 \times 10^{-1}$	$4.608 \times 10^{-5}$	$1.535 \times 10^{-5}$	$6.777 \times 10^{-3}$	$7.972 \times 10^{-4}$
11	$1.860 \times 10^{-1}$	$3.335 \times 10^{-5}$	$6.505 \times 10^{-6}$	$4.198 \times 10^{-2}$	$1.855 \times 10^{-3}$

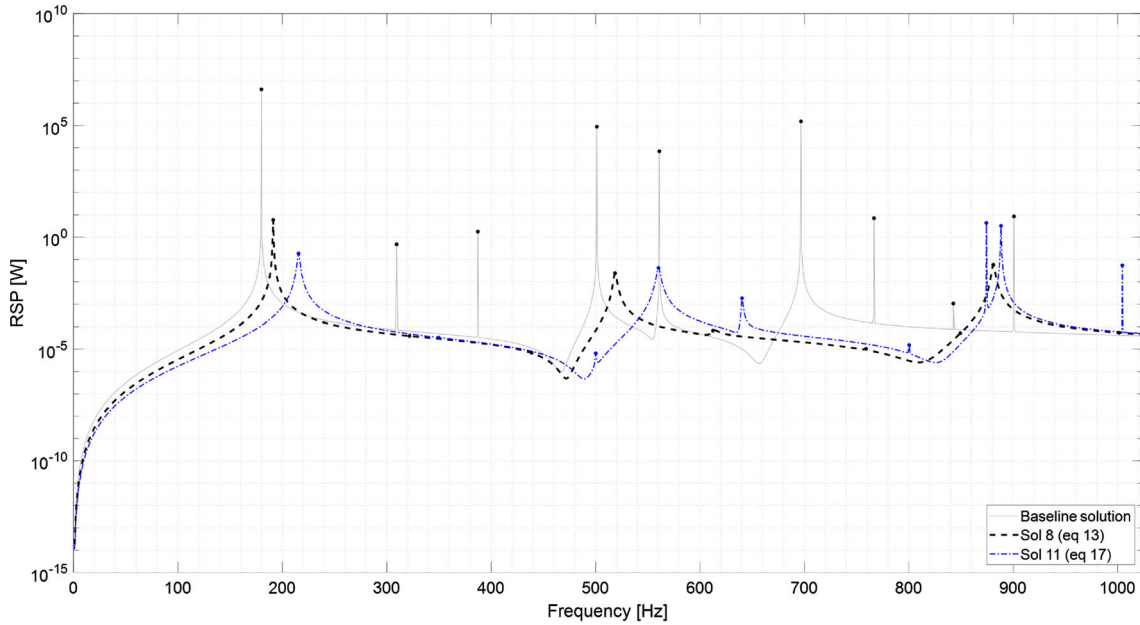


**Fig. 14** RSP curves for solution 9 (Fig. 10) and for solution 11 (Fig. 13)

Figure 16 displays the RSP curves of the best solution in terms of noise attenuation obtained from problem (17) and the one with the best solution obtained in the previous work [15]. It is important to highlight that the piezoelectric material and the interval of the resistances used in each work was different. Still, we can see that both approaches were able to generate solutions that can reduce the targeted modes to similar levels.

As for the computational efforts between both works, it should be of the same order of magnitude as the same optimization algorithm is used.

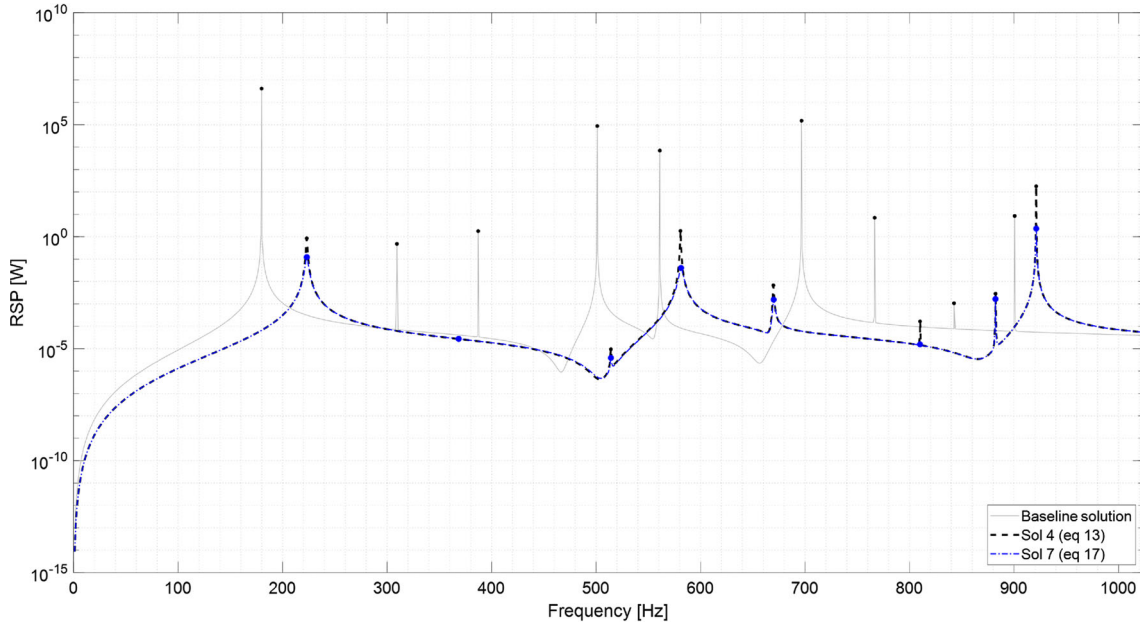


Fig. 15 RSP curves for solution 10 (Fig. 10) and for solution 5 (Fig. 13)

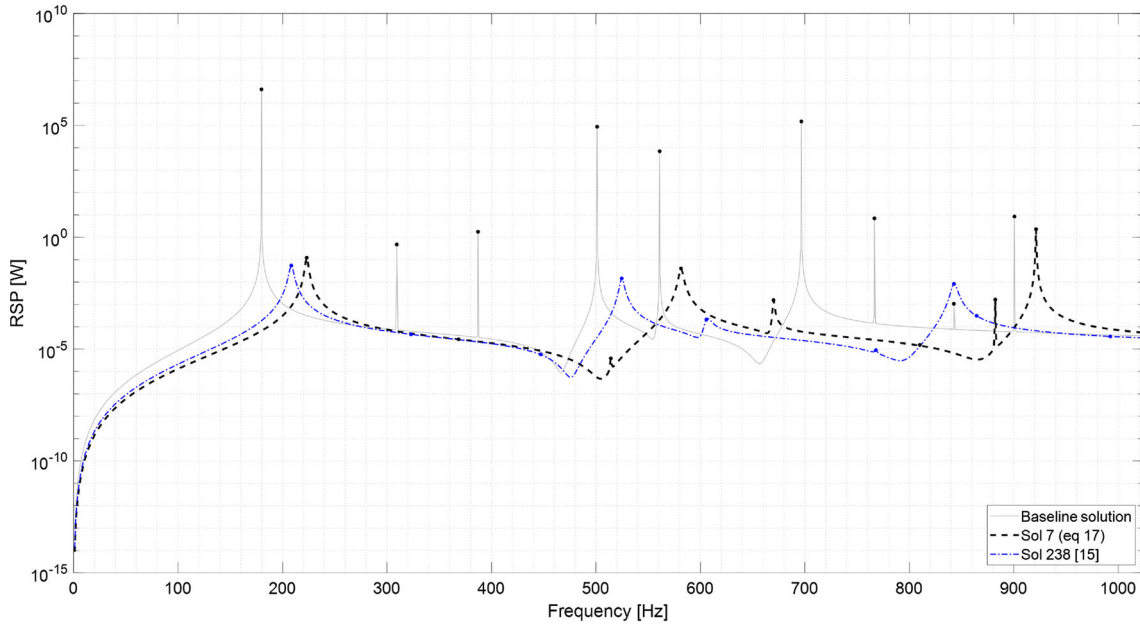


Fig. 16 RSP curves for the best solution (sol. 4) obtained in problem (17) and the best solution obtained in the previous work [15] in terms of maximum damping

### 6 Conclusions

This paper addressed the issue of noise reduction of laminated sandwich panels with a viscoelastic core and surface-bonded piezoelectric patches with purely resistive shunted damping networks. The RSP was evaluated from Rayleigh’s integral. A multi-objective optimization problem was solved in order to obtain the optimal position of the piezoelectric patches in order to reduce the radiated noise in the first five modes. As such, seven objectives were considered: minimize the added mass, minimize the number of resistive circuits needed (by minimizing the number of equipotential zones) and the RSP response amplitudes of the first five modes. In the end, the norm of  $L_1$  was used to compare the responses of each solution. This methodology was proven

in order to obtain the configuration of the patches that reduce the overall response of the panel within the considered frequency range. To finish the optimization process, the comparison criterion used to rank the best solutions for the five modes, norm of  $L_1$ , is used as an objective. In other words, we end the optimization process with the resolution of a multi-objective problem with three objectives (replacing from the problem with seven objectives the last five objectives, which correspond to the first five modes, by a single objective, the norm of  $L_1$ , while keeping the first two). Another relevant aspect to point out is that no inductances were used in this work. As such, the influence of the inductances in the problem presented here could be an important issue to address in a future work.

**Acknowledgements** This work has been supported by National Funds through Fundação para a Ciência e Tecnologia (FCT), through IDMEC, under LAETA, project UID/50022/2020.

### Declarations

**Conflict of interest** The authors declare no conflict of interest in preparing this article.

### References

1. Baz, A.M.: Active and Passive Vibration Damping, 1st edn. Wiley, Hoboken (2019). Online ISBN:9781118537619
2. Forward, R.L.: Electronic damping of vibrations in optical structures. *Appl. Opt.* **18**(5), 690–697 (1979). <https://doi.org/10.1364/AO.18.000690>
3. Hagood, N.W., von Flotow, A.: Damping of structural vibrations with piezoelectric materials and passive electrical networks. *J. Sound Vib.* **146**(2), 243–268 (1991). [https://doi.org/10.1016/0022-460X\(91\)90762-9](https://doi.org/10.1016/0022-460X(91)90762-9)
4. Wu, S.Y.: Piezoelectric shunts with a parallel R–L circuit for structural damping and vibration control. In: Johnson, C.D. (ed.) *Smart Structures and Materials 1996: Passive Damping and Isolation*, vol. 2720, pp. 259–269. SPIE, San Diego (1996). <https://doi.org/10.1117/12.239093>. International Society for Optics and Photonics
5. Tang, J., Wang, K.W.: Active-passive hybrid piezoelectric networks for vibration control: comparisons and improvement. *Smart Mater. Struct.* **10**(4), 794–806 (2001). <https://doi.org/10.1088/0964-1726/10/4/325>
6. Toftekær, J.F., Benjeddou, A., Høgsberg, J., Krenk, S.: Optimal piezoelectric resistive-inductive shunt damping of plates with residual mode correction. *J. Intell. Mater. Syst. Struct.* **29**(16), 3346–3370 (2018). <https://doi.org/10.1177/1045389X18798953>
7. Larbi, W., Deü, J.-F., Ohayon, R.: Finite element formulation of smart piezoelectric composite plates coupled with acoustic fluid. *Compos. Struct.* **94**(2), 501–509 (2012). <https://doi.org/10.1016/j.compstruct.2011.08.010>
8. Larbi, W., Deü, J.-F., Ohayon, R.: Finite element reduced order model for noise and vibration reduction of double sandwich panels using shunted piezoelectric patches. *Appl. Acoust.* **108**, 40–49 (2016). <https://doi.org/10.1016/j.apacoust.2015.08.021>
9. Larbi, W., Deü, J.-F., Ohayon, R.: Vibroacoustic analysis of double-wall sandwich panels with viscoelastic core. *Comput. Struct.* **174**, 92–103 (2016). <https://doi.org/10.1016/j.compstruc.2015.09.012>
10. Larbi, W., Silva, L., Deü, J.-F.: An efficient FE approach for attenuation of acoustic radiation of thin structures by using passive shunted piezoelectric systems. *Appl. Acoust.* **128**, 3–13 (2017). <https://doi.org/10.1016/j.apacoust.2017.04.013>
11. Larbi, W.: Numerical modeling of sound and vibration reduction using viscoelastic materials and shunted piezoelectric patches. *Comput. Struct.* **2**, 32 (2017). <https://doi.org/10.1016/j.compstruc.2017.07.024>
12. Larbi, W., Deü, J.-F., Silva, L.: Design of shunted piezoelectric patches using topology optimization for noise and vibration attenuation **5**, 23–33 (2017). [https://doi.org/10.1007/978-3-319-41459-1\\_3](https://doi.org/10.1007/978-3-319-41459-1_3). ISBN: 978-3-319-41458-4
13. Vieira, F.S., Araújo, A.L.: Optimization and modelling methodologies for electro-viscoelastic sandwich design for noise reduction. *Compos. Struct.* **235**, 111778 (2020). <https://doi.org/10.1016/j.compstruct.2019.111778>
14. Vieira, F.S., Araújo, A.L.: Implementation of a PID controller in ANSYS for noise reduction applications. *Mech. Adv. Mater. Struct.* **28**(15), 1579–1587 (2021). <https://doi.org/10.1080/15376494.2019.1690721>
15. Araújo, A.L., Madeira, J.F.A.: Optimal passive shunted damping configurations for noise reduction in sandwich panels. *J. Vib. Control* **26**(13–14), 1110–1118 (2020). <https://doi.org/10.1177/1077546320910542>
16. Custodio, A.L., Madeira, J.F.A., Vaz, A.I.F., Vicente, L.N.: Direct multiobjective optimization. *SIAM J. Optim.* **21**(3), 1109–1140 (2011). <https://doi.org/10.1137/10079731X>
17. Madeira, J.F.A., Araújo, A.L., Mota Soares, C.M., Mota Soares, C.A.: Multiobjective optimization of viscoelastic laminated sandwich structures using the direct multiobjective search method. *Comput. Struct.* **147**, 229–235 (2015). <https://doi.org/10.1016/j.compstruc.2014.09.009>
18. Madeira, J.F.A., Araújo, A.L., Soares, C.M.M., Soares, C.A.M., Ferreira, A.J.M.: Multiobjective design of viscoelastic laminated composite sandwich panels. *Compos. Part B: Eng.* **77**, 391–401 (2015). <https://doi.org/10.1016/j.compositesb.2015.03.025>
19. Araújo, A.L., Carvalho, V.S., Mota Soares, C.M., Belinha, J., Ferreira, A.J.M.: Vibration analysis of laminated soft core sandwich plates with piezoelectric sensors and actuators. *Compos. Struct.* **151**, 91–98 (2016). <https://doi.org/10.1016/j.compstruct.2016.03.013>
20. Araújo, A.L., Lopes, H.M.R., Vaz, M.A.P., Mota Soares, C.M., Herskovits, J., Pedersen, P.: Parameter estimation in active plate structures. *Comput. Struct.* **84**, 1471–1479 (2006). <https://doi.org/10.1016/j.compstruc.2006.01.017>



21. Reddy, J.N.: *Mechanics of Laminated Composite Plates and Shells: Theory and Analysis*, Second Edition. CRC Press, Boca Raton (2003). ISBN: 9780203502808
22. Christensen, R.M.: *Theory of Viscoelasticity: An Introduction*. Elsevier Science, New York, NY (2012). ISBN: 9780323161824
23. Sorensen, D.C.: Implicitly restarted Arnoldi/Lanczos methods for large scale eigenvalue calculations, Technical Report tr95-13 edn. Department of Computational and Applied Mathematics. Houston, Texas: Rice University, (1995)
24. Fahy, F., Gardonio, P.: *Sound and Structural Vibration*. Elsevier Science, Oxford (2007). ISBN: 9780080471105
25. Pritz, T.: Five-parameter fractional derivative model for polymeric damping materials. *J. Sound Vib.* **265**(5), 935–952 (2003). [https://doi.org/10.1016/S0022-460X\(02\)01530-4](https://doi.org/10.1016/S0022-460X(02)01530-4)
26. eFunda Portal: Lead Zirconate Titanate (PZT-4). [https://www.efunda.com/materials/piezo/material\\_data/matdata\\_output.cfm?Material\\_ID=PZT-4](https://www.efunda.com/materials/piezo/material_data/matdata_output.cfm?Material_ID=PZT-4). Last accessed: 08 Nov 2021
27. Franco Correia, V.M., Madeira, J.F.A., Araújo, A.L., Mota Soares, C.M.: Multiobjective design optimization of laminated composite plates with piezoelectric layers. *Compos. Struct.* **169**, 10–20 (2017). <https://doi.org/10.1016/j.compstruct.2016.09.052>

**Publisher's Note** Springer Nature remains neutral with regard to jurisdictional claims in published maps and institutional affiliations.

Springer Nature or its licensor (e.g. a society or other partner) holds exclusive rights to this article under a publishing agreement with the author(s) or other rightsholder(s); author self-archiving of the accepted manuscript version of this article is solely governed by the terms of such publishing agreement and applicable law.